

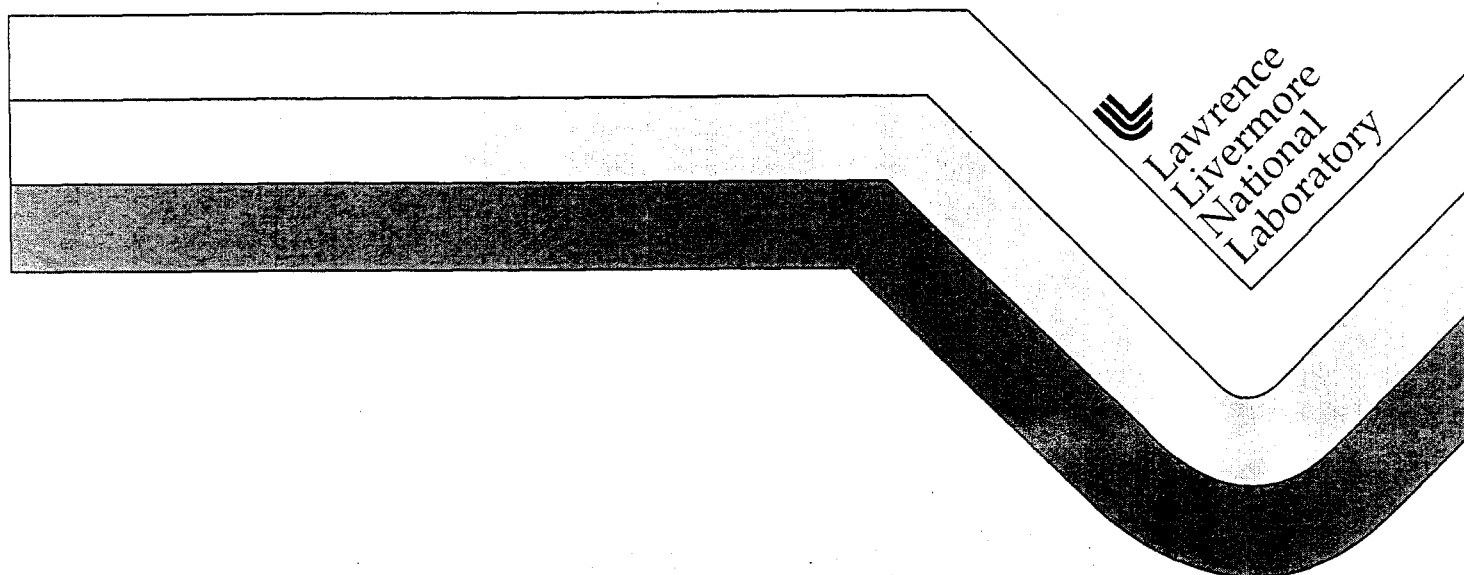
# Computational Simulations of High Intensity X-Ray Matter Interaction

**Richard A. London, R.M. Bionta**  
**Lawrence Livermore National Laboratory**

**R.O. Tatchyn and S. Roesler**  
**Stanford Synchrotron Radiation University**

This paper was prepared for submittal to  
SPIE Conference on Optics for Fourth Generation X-Ray Sources

August 2, 2001



## **DISCLAIMER**

This document was prepared as an account of work sponsored by an agency of the United States Government. Neither the United States Government nor the University of California nor any of their employees, makes any warranty, express or implied, or assumes any legal liability or responsibility for the accuracy, completeness, or usefulness of any information, apparatus, product, or process disclosed, or represents that its use would not infringe privately owned rights. reference herein to any specific commercial products, process, or service by trade name, trademark, manufacturer, or otherwise, does not necessarily constitute or imply its endorsement, recommendation, or favoring by the United States Government or the University of California. The views and opinions of authors expressed herein do not necessarily state or reflect those of the United States Government or the University of California, and shall not be used for advertising or product endorsement purposes.

# Computational Simulations of High Intensity X-Ray Matter Interaction

R. A. London\* and R. M. Bionta  
Lawrence Livermore National Laboratory

R. O. Tatchyn and S. Roesler  
Stanford Synchrotron Radiation Laboratory

## ABSTRACT

Free electron lasers have the promise of producing extremely high-intensity short pulses of coherent, monochromatic radiation in the 1-10 keV energy range. For example, the Linac Coherent Light Source at Stanford is being designed to produce an output intensity of  $2 \times 10^{14}$  W/cm<sup>2</sup> in a 230 fs pulse. These sources will open the door to many novel research studies. However, the intense x-ray pulses may damage the optical components necessary for studying and controlling the output. At the full output intensity, the dose to optical components at normal incidence ranges from 1-10 eV/atom for low-Z materials ( $Z < 14$ ) at photon energies of 1 keV. It is important to have an understanding of the effects of such high doses in order to specify the composition, placement, and orientation of optical components, such as mirrors and monochromators. Doses of 10 eV/atom are certainly unacceptable since they will lead to ablation of the surface of the optical components. However, it is not precisely known what the damage thresholds are for the materials being considered for optical components for x-ray free electron lasers. In this paper, we present analytic estimates and computational simulations of the effects of high-intensity x-ray pulses on materials. We outline guidelines for the maximum dose to various materials and discuss implications for the design of optical components.

keywords: x-ray lasers, free-electron lasers, x-ray optics, computer simulation

## 1. INTRODUCTION

Optical components may be damaged by the extremely high pulsed fluence of x-ray free electron lasers (XFELs). In order to design robust optics we need to understand the fundamental damage mechanisms and determine the threshold x-ray fluence to cause damage. The mechanisms and thresholds depend on the materials and structure of the components and the angle of incidence of the x-ray beam. We are interested in several types of optical elements: collimators, attenuators (gas cell or foil), deflection mirrors, focusing elements (reflection, Fresnel), monochromators (crystal, reflective) and beam stops.

Our work is specifically aimed at the design of optics for the Linac Coherent Light Source (LCLS), proposed to be built at the Stanford Linear Accelerator Center.<sup>1</sup> The current design has two experimental halls. The near hall extends 30 m to 100 m from the end of the undulator. A second (far) hall is proposed beginning at 250 m from the end of the undulator, to allow the beam to expand thus

---

\* Contact: [rlondon@llnl.gov](mailto:rlondon@llnl.gov); (925) 423-2021; L-30, Lawrence Livermore National Laboratory, Livermore, CA 94550.

lessening the fluence on the optics. Our main concern is in the near hall. A primary determinant of the effect of x rays on materials is the incident fluence (energy/area). The fluence of the unfocused beam can be estimated from the electron beam width assuming a coherent gaussian x ray beam.<sup>2</sup> Fluences expected from the LCLS are shown in Figure 1. The fluence decreases with distance from the undulator due to diffraction. The decrease is faster at lower photon energies.

The nature of the damage problem can be understood by estimating the dose to materials placed near the end of the undulator as shown in Figure 2.<sup>2</sup> The dose represents the average energy per atom deposited in the near-surface region of a component exposed to a single x-ray laser pulse. The doses have been calculated from the fluences as shown in Figure 1 and tabulated x-ray absorption coefficients,<sup>3</sup> assuming that the absorbed x-ray energy is locally thermalized. This is expected to be accurate for all situations except grazing incidence optics in which case electron transport may spread out the absorbed energy and lower the dose (see section 5).

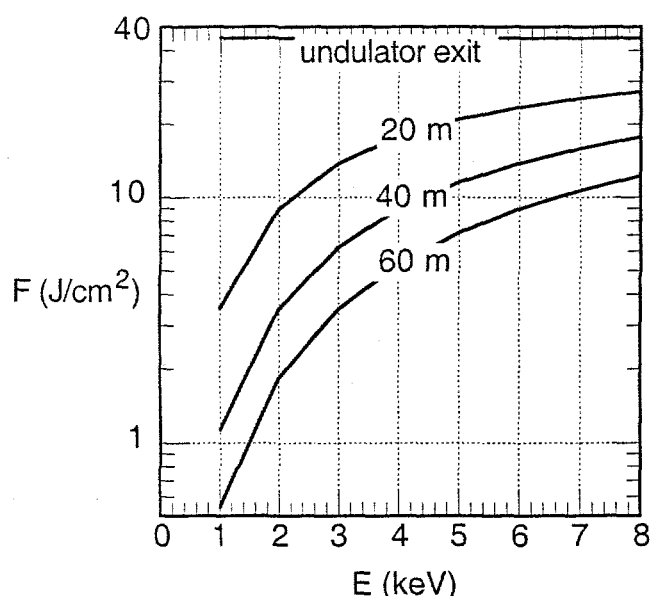


Figure 1. Fluence versus photon energy at several distances from the LCLS undulator exit. The fluence is calculated for a gaussian beam with waist diameter of  $33 \mu\text{m}$  and an energy of 2.3 mJ.

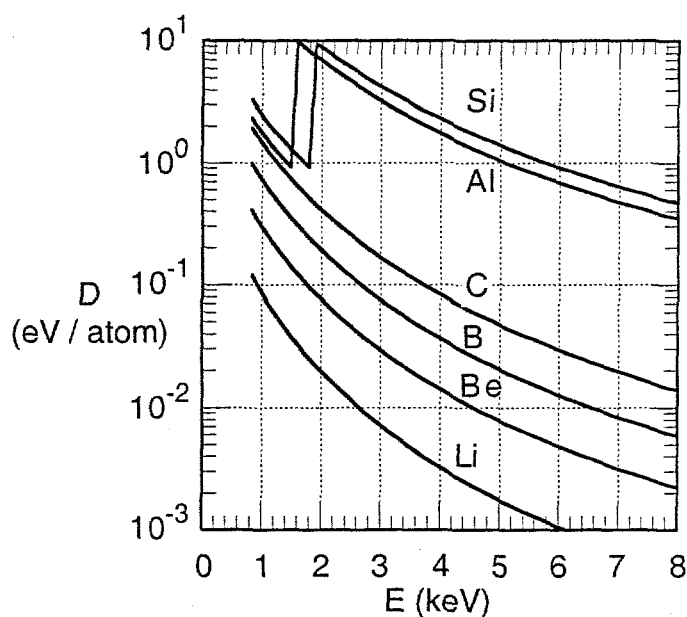


Figure 2. Dose versus photon energy for several low-Z materials, at 15 m from the LCLS undulator.

We focus on the single-pulse dose, since the average power loading of x-ray FELs is generally small comparing to existing light sources and the standard methods for removing the time-averaged absorbed power can be applied. Since typical binding energies of materials are 1 eV/atom, doses approaching this level (say  $> 0.1$  eV/atom) should be viewed as possibly damaging. We see that the dose generally decreases with increasing photon energy between 1 and 8 keV, and increases with increasing atom number. All of the solid elements may receive doses larger than 0.1 eV near the undulator exit, and only the lightest elements have a chance of receiving doses below 1 eV/atom.

## 2. FUNDAMENTAL PROCESSES

### 2.1 X-ray and electron processes

To understand the effect of short pulse, high intensity x-ray pulses on matter we start by looking at the fundamental x-ray and electron processes, shown in Figure 3. The x rays are absorbed mainly by inner-shell photoionization. For light atoms ( $Z < 30$ ) the core-excited ions relax primarily by Auger decay, in which the core hole is filled by an outer shell electron, with the extra energy going to the ionization of a second outer shell electron. This leaves the ion with 2 (or more for higher  $Z$  elements) valence shell holes. The Auger processes take approximately 10 fs. The free electrons then undergo slowing by ionization and collisions with free electrons, especially in conductors in which there are many free electrons. Thermalization of the photo-ionized and Auger electrons is expected to take approximately 20 fs. On much longer timescales ( $\sim 1$  to 10 ps) the electrons will thermalize with the ions and neutral atoms in the material and then finally recombine with the ions.

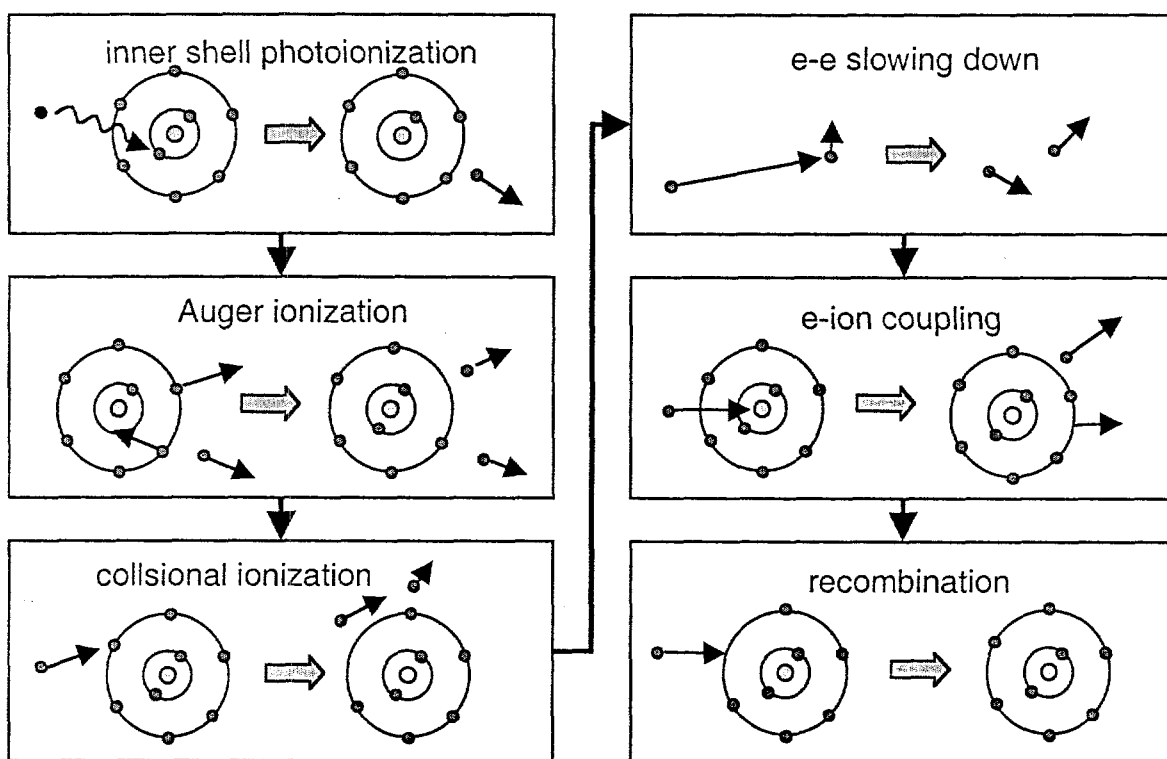


Figure 3. The fundamental processes of x-ray and electron interaction within materials.

### 2.2 Implications of optical laser-matter interaction experiments

Recent experiments on optical laser-matter interaction shed light on many of the electron and ion processes which we expect to take place in the x-ray case, once the electrons have slowed down. These experiments have measured the time evolution of the free electron density, both thermal and non-thermal coupling of electron energy to ions, and the final state of the matter, under illumination at various fluences. The group in Essen has done extensive experiments in silicon.<sup>4</sup> They observe melting at a fluence of about  $0.17 \text{ J/cm}^2$  for 630 nm light in 130 fs pulses. Given the measured absorption coefficient, this corresponds to a dose of about  $0.64 \text{ eV/atom}$ , close to the expected melting dose based on the thermodynamics of silicon. They see permanent damage only at higher fluences. The Berkeley

group has studied the generation of stress waves in InSb with ultrashort pulses.<sup>5</sup> They observe non-thermal coupling of the electron energy to the lattice on timescales less than 10 ps, for fluences near the melting point. They see permanent damage (discoloration) of the material slightly below the melt fluence of 0.13 eV/atom. The group in San Diego<sup>6</sup> did experiments in Ge, in which they observe non-thermal fast melting at rather high doses (4.5 eV/atom).

These experiments have several implications for understanding intense x-ray laser-matter interaction. 1) Thermal (i.e. collisional) coupling of electrons to ions takes place in approximately 10 ps. Processes such as generation of stress waves and normal melting generally take place after this time. 2) Non-thermal coupling of the electrons to ions may take place much faster. Most of the observations pertaining to this are at high fluences (above melt). 3) Damage is not observed for fluences much less than the melt fluence. Many of the time dependent effects associated with few eV electrons are likely to be similar to the x-ray case.

### 2.3 Energy-time view of processes

Combining the fundamental x-ray processes illustrated in Figure 3, and the results of the optical laser-matter interaction experiments leads to a qualitative energy-time picture of the x-ray interaction shown in Figure 4. The processes of major concern for the operation of the x-ray optical components are outlined with bold lines. They involve motion of the ions since most of the electrons remain attached to ions.

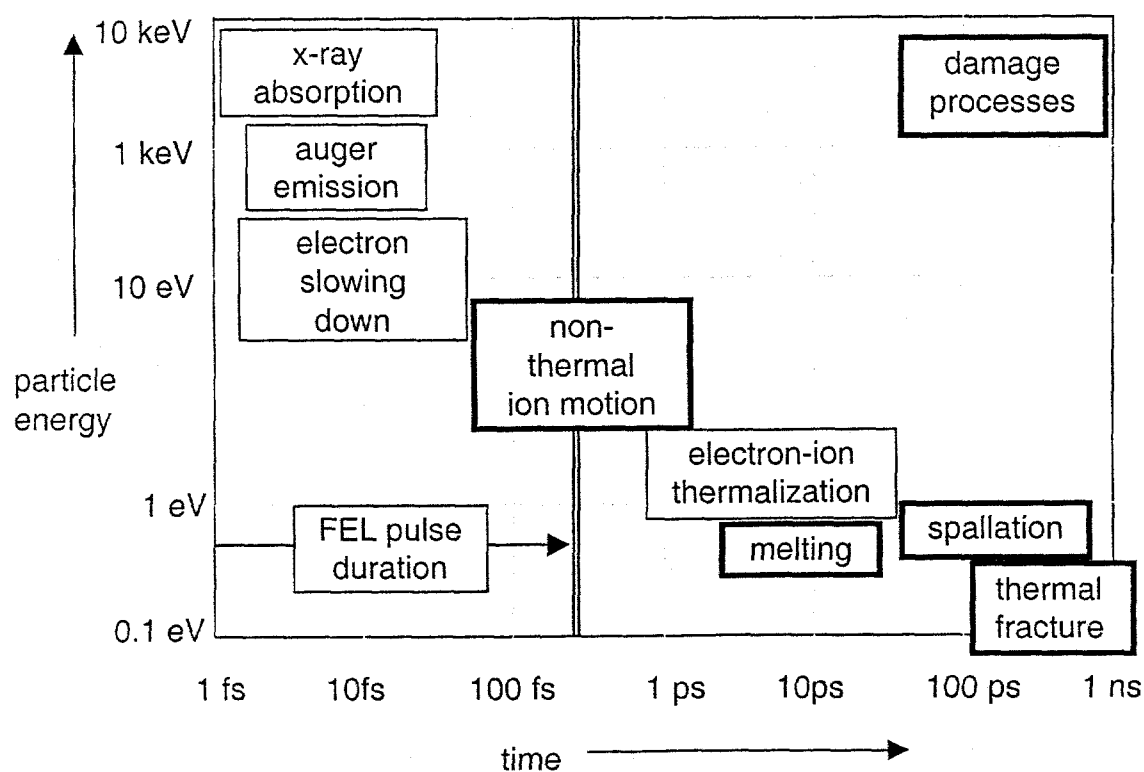


Figure 4. Energy-time plot of processes associated with high intensity x-ray-matter interaction.

## 2.4 Damage thresholds

Table 1 summarizes properties of several low-Z materials, and estimated doses for melting and spallation, the two primary permanent damage mechanisms which we believe will set a maximum allowable dose. The melt temperatures and doses are from the Handbook of Chemistry and Physics,<sup>7</sup> while the spallation pressures and doses are from the various references listed. The melting doses are in the range 1/3 - 1 eV/atom. It is important to note the recent spallation results of Moshe et al.<sup>8</sup> They found that for short stress pulses, which they generated with 80 ps optical laser pulses, the spallation thresholds much higher than the typical values derived from long pulse experiments. It appears that materials can withstand higher tensile stresses when these are applied only for very short periods of time. This is expected to be the case for the FEL x-ray pulses, so that the higher spallation thresholds are likely to apply.

Table. Damage thresholds for low-Z materials

Material	Be	C	Al	Si	B <sub>4</sub> C
Quantity					
T <sub>melt</sub> (K)	1560	3800	930	1690	2620
D <sub>melt</sub> (eV/atom)	0.43	0.9	0.30	0.87	0.62
P <sub>s, long pulse</sub> (kbar)	8 <sup>9</sup>		12 <sup>9</sup>		
D <sub>s, long pulse</sub>	0.15		0.12		
P <sub>s, short pulse</sub>			80 <sup>8</sup>		
D <sub>s, short pulse</sub>			0.88		

## 3. COMPUTATIONAL MODELING METHODS

The categorization of the fundamental processes in Figure 4 leads to a natural division of the modeling problem into three parts. The first part is to model the fundamental x-ray and high energy electron interactions. For this part of the modeling, the Monte Carlo method is preferred. In this method, the paths of photons and electron are simulated in a probabilistic manner. A large number of initial photons ( $\sim 10^4$  to  $10^6$ ), and the resultant photoelectrons and secondary electrons are tracked in energy, space, and time. This produces a quantitative description of the distribution of the particles and ultimately a space and time dependent distribution of dose. To a good approximation we can assume that the interaction cross sections for x-rays and electrons are constant during the x-ray pulse, being given by the values for cold material. This is valid since the x rays interact mainly with inner shell electrons, and the fraction of the atoms with inner shell holes is very small, less than about 0.1% for doses less than 1 eV/atom. The high energy electron slowing down is also not altered much by the small amount of ionization that occurs during the pulse. This assumption is expected to be accurate for following the electrons down to energies of around 100-200 eV. At this point the interaction cross sections are so strong that the electrons are expected to remain localized.

In order to carry the simulation further we require more exact treatment of the electron interaction since the detailed structure of the material and the excitation and ionization of the atom valence shells will be important. In addition, for certain applications such as crystal diffraction, it is important to model the motion of the ions. We suggest that the method of molecular dynamics, including electron and ion dynamics, is the best way to model the intermediate energy and timescale events shown in Figure 4. Several calculations of optical laser-matter interaction illustrate the value of this method.<sup>10</sup> The main goal of molecular dynamics method is to calculate ion motion on a relatively short time scale—on the order of the x-ray pulse duration. Both non-thermal and thermal processes may cause ion motion. Non-thermal processes are caused by collective electrostatic forces resulting from changes in the electron spatial distribution. These are expected when a significant fraction (>10%) of the valence shell electrons are excited or ionized. For very high fluence ultra-short pulse optical excitation, non-thermal melting of the lattice can occur on very short time scales (< 200 fs). Thermal motion of the ions is caused by electron-ion coupling. Generally the timescale for this process is of order 10 ps, so we do not expect much thermal ion motion during the pulse.

Ultimately thermal ion motion can produce long term damage by mechanisms such as melting, spallation, or cracking. These processes can be modeled by hydrodynamic, (i.e. continuum mechanics) methods. The hydrodynamic methods can be applied once the electrons thermalize, and can accurately describe effects such as the formation of stress waves, and the resultant processes of spallation and shear fracture. Several computer programs exist with the capability for relevant hydrodynamic modeling.

To date we have performed Monte Carlo simulations of the early time x-ray and electron processes, and hydrodynamic simulations of the late time thermal processes. We plan to implement molecular dynamic simulations in the future. In the next section (§4) we discuss the calculation of dose for the special case of grazing incidence optics, including Monte Carlo calculations. We then discuss hydrodynamic simulations for grazing incidence optics and transmissive diffractive optics in §5.

## 4. DOSE TO GRAZING INCIDENCE OPTICS

Grazing incidence mirrors can be used for filtering, redirecting and/or focusing the x-ray beam. They are attractive because they can achieve high reflectivity and low dose. In grazing incidence, the penetration of the x rays into the material is quite small so that the transport of photo-electrons may lower the dose by spreading it to deeper layers of the material. In this section, we make analytic estimates of the dose for grazing incidence optics and also illustrate the use of the Monte Carlo method for more accurate calculations.

### 4.1 Analytic estimate of dose

An estimate of the energy penetration depth may be made from the following formula:

$$d_{en} = \max[d_x, \min(d_{coll}, d_{elec})], \quad (1)$$

where  $d_x$  is the x-ray penetration distance,  $d_{coll}$  the electron collisional range and  $d_{elec}$  the electrostatic range of the electrons, set by the charge which may build up in the irradiated layer as a large number of electrons attempt to leave the thin layer in short period of time.

The x-ray penetration distance is determined from a solution of Maxwell equations for a wave incident from vacuum onto a medium of complex index of refraction:

$$d_x = \frac{\lambda \rho}{4\pi\beta}, \text{ where } \rho = \sqrt{\frac{1}{2} \left[ \sin^2 \theta - 2\delta + \sqrt{(\sin^2 \theta - 2\delta)^2 + 4\beta^2} \right]}. \quad (2)$$

Here  $\lambda$  is the photon wavelength, and  $\delta$  and  $\beta$  are the real and imaginary optical constants.<sup>3</sup> Figure 5 shows the x-ray penetration distance for 1 keV photons for three materials, Be, C and Si. For each material, there exists a critical angle given by  $\theta_{crit} = \sqrt{2}$ , characterizing the x-ray penetration. For angles much less than the critical angle, the mirror becomes highly reflective, and the penetration depth becomes approximately constant at a value of  $3 \times 10^{-3} \mu\text{m}$ . The penetration depth rises rapidly as the angle increases past the critical value, and becomes proportional to  $\sin(\theta)$  at larger angles.

The dose for grazing angles may be estimated from the fluence, the angle of incidence, the reflectivity [found from the electromagnetic analysis behind Eq. (2)], and a formula for the electron collisional range.<sup>11</sup> In calculating the dose we assume that the Auger electrons deposit their energy locally, since they have much lower energy (and range) than the photoelectrons. Figure 6 shows the dose estimated for low-Z materials 80 m from the end of the LCLS undulator. This position and energy are chosen for proposed atomic physics experiments, in which grazing incidence optics will be used to filter and focus the x rays. Figure 6a shows the large effect of electron transport in lowering the dose at small angles. Figure 6b shows that the expected dose increases with atomic number and with angle below the critical value. Above the critical angle, the dose approaches a constant value for each material. Angles of around 1 deg appear to produce reasonable doses ( $\ll 1$  eV/atom).

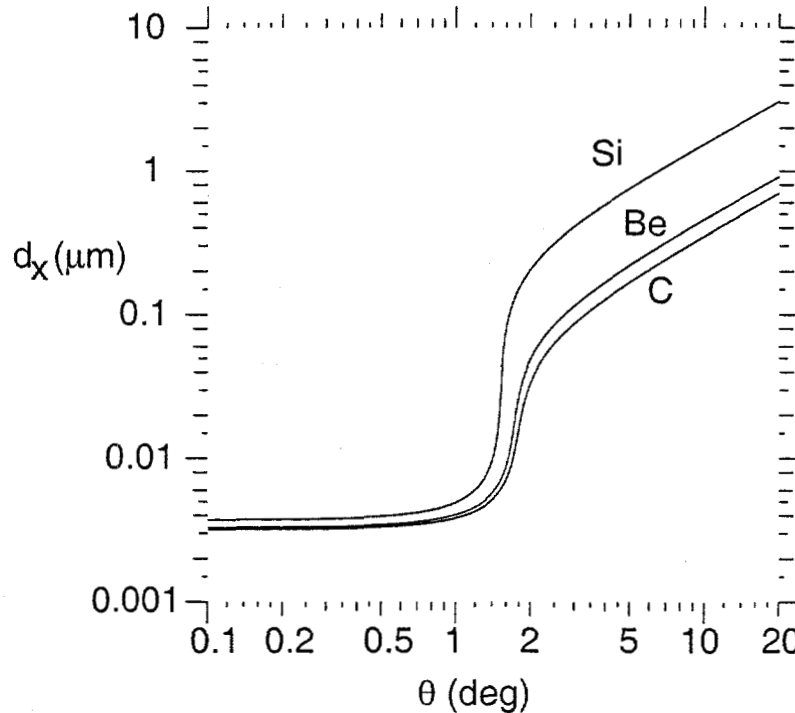


Figure 5. Penetration depth (normal to the surface) for 1 keV x rays incident at grazing angles. The critical angles are 1.52, 1.78, and 1.71 deg for Be, C, and Si, respectively.

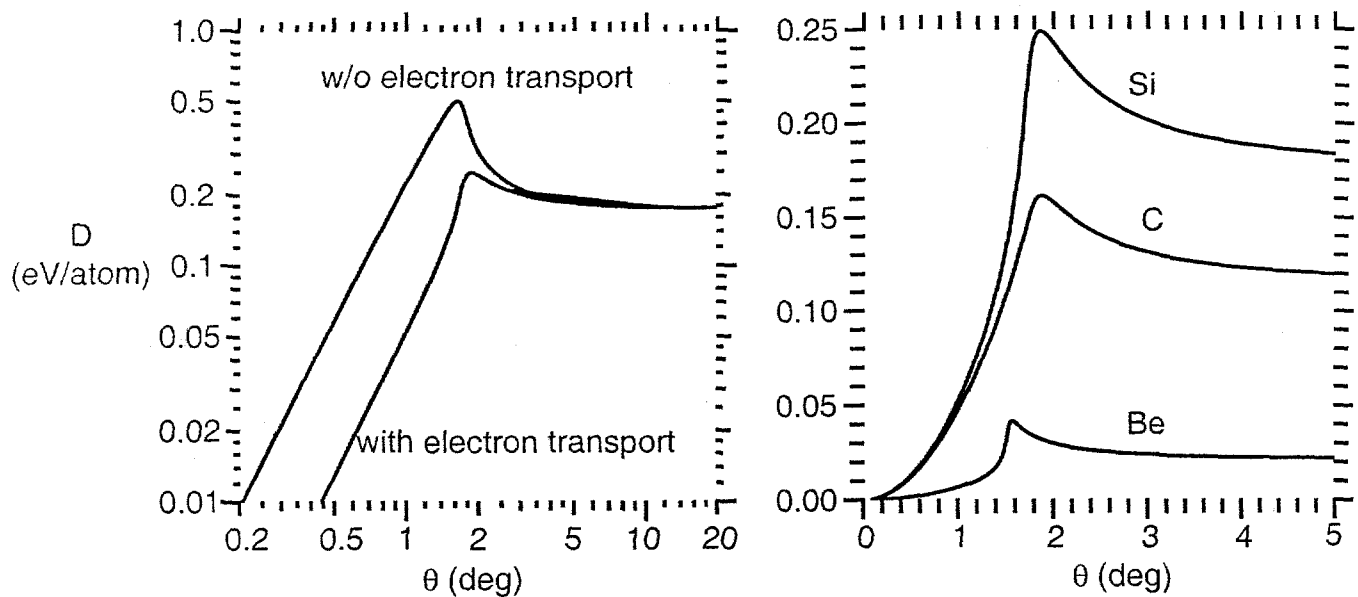


Figure 6. Dose estimated from x-ray penetration depth and electron range. a) shows dose with and without electron transport for Si, 6b shows dose for Be, C and Si, all including electron transport.

#### 4.2 Monte Carlo simulations of dose

In order to improve upon the dose estimates given above and ultimately to study more complicated situations such as multi-layer mirrors, we have begun Monte Carlo calculations. Two widely available programs have been used—FLUKA,<sup>12</sup> and Penelope.<sup>13</sup> Figure 7a shows very close agreement in the spatial dependence of the dose between the two programs. The Fluka results are somewhat smoother since more particles were used ( $10^6$  vs.  $10^4$  for the Penelope results). The fall off in the dose towards the surface is due to escaping electrons. In reality, we do not expect such a large number of escaping electrons because of the charge build-up. Thus the dose is probably underpredicted by the Monte Carlo programs near the surface. In the future we plan to include electrostatic forces to account for this effect. Using the Penelope program, we show the spatial dependence of the dose expected for the atomic physics experiment mirrors in Figure 7b. The doses predicted here are of the same order of magnitude, but somewhat smaller than the analytic estimates given in Figure 6. There are two reasons for the difference. First is the escape of electrons present in the Monte Carlo calculations. Second is the fact that the Monte Carlo program tracks the Auger electrons, which were assumed to be locally stopped in the analytic estimates. Since the escape of electrons is believed to be incorrect in the Monte Carlo simulations, the true surface doses are expected to be about  $10^{-2}$ ,  $3 \times 10^{-2}$  and to  $5 \times 10^{-2}$  for Be, C and Si, respectively. Since these doses are well below the melting and spallation thresholds listed in Table 1, they are not likely to be damaging.

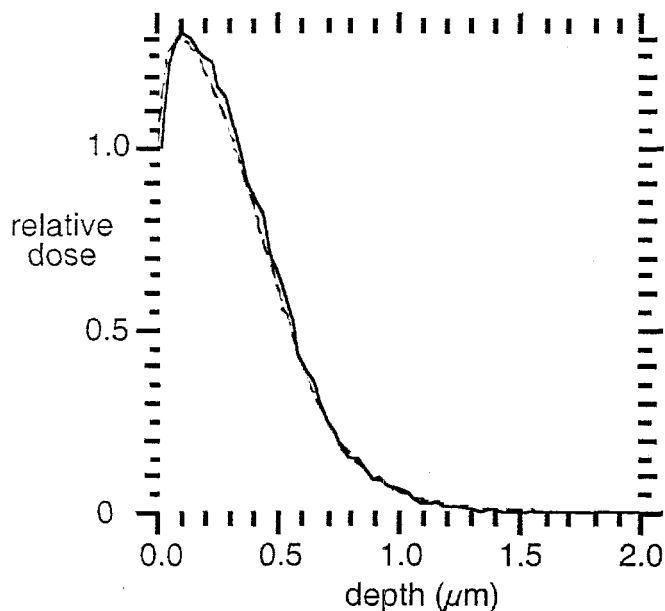


Figure 7a. The dose calculated by Penelope (solid curve) and Fluka (dashed curve) are in good agreement. Calculations are for 6 keV photons incident on Be at 1 degree grazing angle.

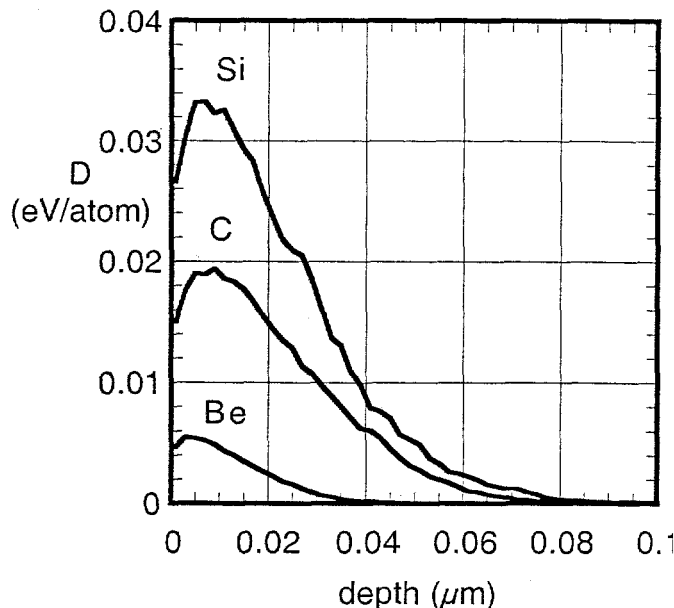


Figure 7b. Dose distribution versus depth for Be, C and Si. The mirror is 80m from the end of the undulator. The x-ray energy is 1 keV and the angle of incidence is 1 deg.

## 5. HYDRODYNAMIC SIMULATIONS

### 5.1 Grazing incidence mirror

To study the long time ( $> \text{ps}$ ) effects of x-ray heating we have performed hydrodynamic simulations, using the LASNEX<sup>14</sup> program. Figure 8 shows results for 2 keV photons incident on a Si mirror. The calculations are one-dimensional, assuming a very large beam width compared to the energy penetration depth. The pulse duration (230 fs) is very short compared to the hydro timescale so that initially we see in Fig. 8a only a large temperature rise, up to 5000 °C at the surface. The temperature decreases with a  $1 \mu\text{m}$  e-folding length into the mirror. The pressure is shown in Fig. 8b at times separated by 50 ps, following the pulse. Initially a high pressure is generated. Stress waves are launched into the mirror and towards the front surface. The wave directed towards the surface is reflected with a reversal in sign, leading to the characteristic bipolar wave seen in the later curves. The density in Fig. 9c shows the propagation of the stress wave into the material, as well as the long-lasting thermal expansion near the surface. The temperature and density relax by heat conduction away from the surface on a much longer timescale, of order 10 ns. The tensile (i.e. negative pressure) component of the stress wave may lead to spallation of the material if the magnitude of the tension exceeds the spall strength. Based on the 80 kbar short-pulse spall strength cited for Al in Table 1, we guess that the peak tension of 35 kbar achieved in this case is not large enough to spall the material. However similar measurements have not been made in Si. The temperature reached near the surface is well above the melting point. Melting will likely lead to 2-dimensional motions (not modeled here) which could cause ripples on the surface upon refreezing, before the next pulse. Therefore, we suggest avoiding the melting of the surface of optics since the surface may become distorted between pulses. At fluence a few times higher, simulations show gas phase ablation of the mirror, clearly an undesirable consequence.

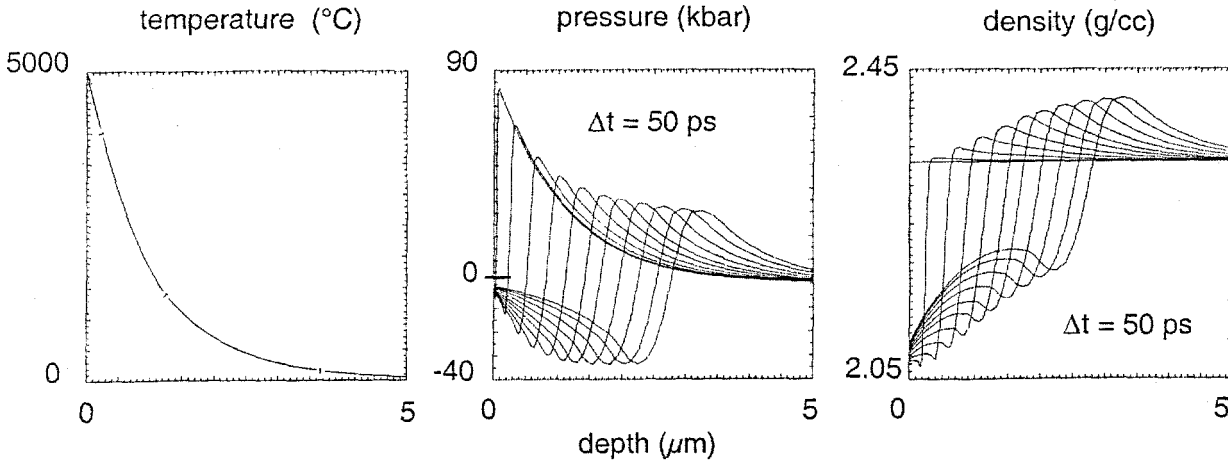


Figure 8. Hydrodynamic simulation of the response of Si mirror to a fluence of  $3 \text{ J/cm}^2$  of 2 keV x rays. This produces a surface dose of 1.25 eV/atom

## 5.2 Fresnel zone plate

We have explored the design, construction, and survivability of Fresnel zone plates, which diffractively focus x rays on transmission. They can be constructed by sputtering alternating layers of two materials onto a rotating wire. Then a piece is sliced out of the cylinder producing a relatively thick zone plate, which can be effective for focusing hard x rays. In Figure 9, we show the hydrodynamic response expected from a Be- $\text{B}_4\text{C}$  zone plate exposed to 8.3 keV x rays. This optic is designed for a warm dense matter experiment on the LCLS. Several approximations have been made in the modeling setup. Although an actual optic would have 50-100 zones, we have modeled only 10 in this calculation. A 1-D slab geometry is assumed, as a good approximation to the thin circular zones. Since the penetration depth of the x rays is large ( $> 1700 \mu\text{m}$ ) compared to thickness of the zone plate ( $33 \mu\text{m}$ ), we have ignored variations in depth. Despite these approximations, we expect the calculations to accurately illustrate the nature of the hydrodynamic effects to be expected in a full optic. As seen in Figure 9, a differential pressure is immediately set up between the Be and  $\text{B}_4\text{C}$  layers, mainly due to their different x-ray absorption coefficients. Motion only begins well after the laser pulse, due to the relatively long sound-crossing time for the  $1/2 \mu\text{m}$  thick layers. The motion causes pressure oscillations with a period of about 140 ps (about  $3/4$  of a period is shown in Figure 9). The peak pressures are about 1.7 kbar, while the peak tensions are 0.6 kbar. We do not expect much damage at these conditions to the internal zones. One concern is that the development of tension between the layers may cause them to separate near the outer radius of the zone plate, since the inter-layer binding strengths may be much lower than the internal strength of either material. This effect can probably be avoided by surrounding the whole zone plate in a tamping material of similar composition.

## 6. SUMMARY AND FUTURE WORK

In this paper we first presented the expected fluences and material doses for the LCLS x-ray free electron laser. We then summarized the understanding of fundamental x-ray and electron processes and the relevant knowledge gained from recent optical laser-matter interaction experiments. This lead to a qualitative picture of the energy flow for the interaction of x-ray FEL pulses with matter. According to

the energy flow picture, a scheme for computational modeling of x-ray-matter interaction consisting of three steps has been proposed. We provided estimates of the damage threshold doses to various low-Z materials for the processes of melting and spallation. We suggest that the process of melting provides a reasonable threshold to guide the design of most optical components.

In order to illustrate the use of computational simulations and to make quantitative statements, we have examined several optical components in detail, including grazing incidence mirrors and Fresnel zone plates. Both analytical and computational calculations are provided for grazing incidence mirrors. We find that by operating below the critical angle, the combination of high reflectivity, large beam footprint, and electron transport combine to produce greatly reduced doses. The design for a mirror to focus 1 keV x rays for atomic physics experiments has comfortably low dose. Hydrodynamic simulations predict fairly high pressures and tensile stresses well after the x ray pulse. However these do not appear to be large enough to cause damage. We then discussed the hydrodynamic response of Fresnel zone plates, designed to focus 8 x rays for warm-dense matter experiments.

Future work will concentrate on completing the computational modeling methods, particularly by adding the molecular dynamics technique to study possible ion motion and associated changes in x-ray diffraction during the x-ray pulse. We will also study special effects on x-ray multi-layer mirrors and the problem of stress concentration in structured Fresnel optics.

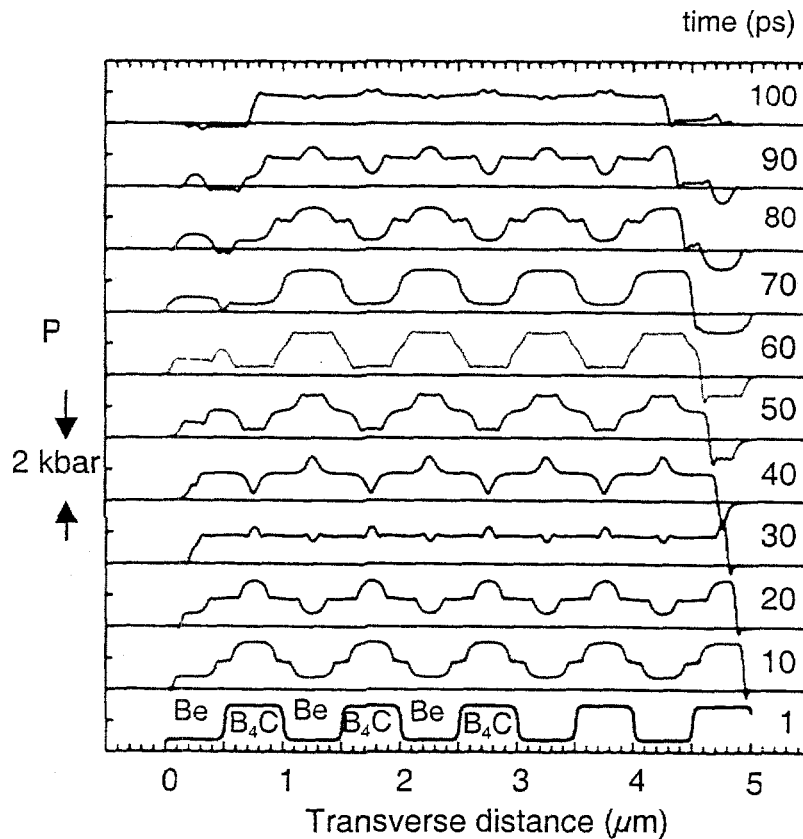


Figure 9. Hydro simulations of a Be/B<sub>4</sub>C Fresnel zone plate irradiated by 8.3 keV x rays. Only 10 layers are modeled. The absorbed doses are 0.002 and 0.007 eV/atom in the Be and B<sub>4</sub>C, respectively. Each time curve is offset, so that the distance between horizontal lines represents 2 kbar pressure.

## ACKNOWLEDGEMENTS

We thank A. Szoke, A. Wootton, and M. Howells for helpful discussions and F. Salvat for making the Penelope program available. This work was performed under the auspices of the U.S. Department of Energy by the University of California Lawrence Livermore National Laboratory under contract No. W-7405-Eng-48.

## REFERENCES

- <sup>1</sup> *Linac Coherent Light Source (LCLS) Design Study Report*, SLAC-R-521, Stanford, CA 1998; available from NTIS, 5285 Port Royal Road, Springfield, VA 22161.
- <sup>2</sup> R. Bionta, "Controlling Dose to Low Z Solids at LCLS," LLNL UCRL-ID-137222, (2000), available at <http://www-ssrl.slac.stanford.edu/lcls/technotes>.
- <sup>3</sup> B. L. Henke, E. M. Gullikson, and J. C. Davis, "X-ray Interactions: Photoabsorption, Scattering, Transmission, and Reflection at E=50-30,000 eV, Z= 1-92", *Atomic Data Nuclear and Data Tables*, **54**, 181-342 (1993), also available at [http://www-cxro.lbl.gov/optical\\_constants/](http://www-cxro.lbl.gov/optical_constants/).
- <sup>4</sup> K. Sokolowski-Tinten and D. von der Linde, "Generation of dense electron-hole plasmas in silicon," *Phys. Rev. B*, **61**, 2643-2650 (2000).
- <sup>5</sup> A. M. Lindenberg et. al., "Time-resolved x-ray diffraction from coherent phonons during a laser-induced phase transition," *Phys. Rev. Lett.*, **84**, 111-114 (2000).
- <sup>6</sup> A. Cavalleri, et. al., "Anharmonic Lattice Dynamics in Germanium Measured with Ultrafast X-ray Diffraction," *Phys. Rev. Lett.*, **85**, 586-589 (2000).
- <sup>7</sup> *Hand Book of Chemistry and Physics, 50th Edition*, R. C. Weast, Ed., The Chemical Rubber Co., Cleveland, 1969, p. D-55.
- <sup>8</sup> E. Moshe et. al, "Experimental measurements of the strength of metals approaching the theoretical limit predicted by the equation of state," *App. Phys. Lett.*, **76**, 1555-1557 (2000).
- <sup>9</sup> D. E. Grady, "The spall strength of condensed matter," *J. Mech. Phys. Solids*, **36**, 353-383 (1988).
- <sup>10</sup> P. L. Silvestrelli, A. Alavi, M. Parrinello, and D. Frenkel, "Structural, dynamical and bonding properties of laser-heated silicon: An ab-initio molecular-dynamics study," *Phys. Rev. B*, **56**, 3806-3812 (1997), A. Gambirasio, M. Bernasconi, and L. Colombo, "Laser-induced melting of silicon: A tight-binding molecular dynamics simulation," *Phys. Rev. B*, **61**, 8233-8237 (2000), H. O. Jeschke, M. E. Garcia, and K. H. Benneman, "Theory for laser-induced ultrafast phase transitions in carbon," *Appl. Phys. A*, **69**, S49-S53 (1999), R. E. Allen, T. Dumitrica, and B. Torralva, "Electronic and structural response of materials to fast intense laser pulses," in *Ultrafast Physical Processes in Semiconductors*, ed: K. T. Tsen (Academic, New York, 2001)
- <sup>11</sup> E. J. Kobetich and R. Katz, "Energy deposition by electron beams and  $\delta$  rays," *Phys. Review*, **170**, 391-396 (1968).
- <sup>12</sup> A. Fasso A. Ferrari, J. Ranft and P. Sala, see <http://fluka.web.cern.ch/fluka>
- <sup>13</sup> F. Salvat, J.M. Fernandez-Varea, J. Baro and J. Sempau, "PENELOPE, An algorithm and computer code for Monte Carlo simulation of electron-photon showers," *Informes Tecnicos Ciemat n. 799* (CIEMAT, Madrid, June 1996), and J. Sempau, E. Acosta, J. Baro , J.M. Fernandez-Varea and F. Salvat, "An algorithm for Monte Carlo simulation of coupled electron-photon transport," *Nucl. Instrum. and Meth.*, **B132**, 377-390 (1997).
- <sup>14</sup> G. B. Zimmerman and W. L. Kruer, *Plasma Phys. Controlled Fusion*, **11**, 82 (1975).